

# Effect of Mn doping on the structural, morphological, optical and magnetic properties of indium tin oxide films

K. M. Reddy · J. Hays · S. Kundu · L. K. Dua ·  
P. K. Biswas · C. Wang · V. Shutthanandan ·  
M. H. Engelhard · X. Mathew · A. Punnoose

Received: 23 November 2006 / Accepted: 3 April 2007  
© Springer Science+Business Media, LLC 2007

**Abstract** We report on the preparation and characterization of high purity manganese (3–9 wt.%) doped indium tin oxide (ITO, In:Sn = 90:10) films deposited by sol–gel mediated dip coating. X-ray diffraction and selected area electron diffraction showed high phase purity cubic  $\text{In}_2\text{O}_3$  and indicated a contraction of the lattice with Mn doping. High-resolution transmission electron microscopy depicted a uniform distribution of ~20 nm sized independent particles and particle induced x-ray emission studies confirmed the actual Mn ion concentration. UV-Vis diffuse reflectance measurements showed band gap energy of 3.75 eV and a high degree of optical transparency (90%) in the 100–500 nm thick ITO films. X-ray photoelectron spectroscopy core level binding energies for In  $3d_{5/2}$  (443.6 eV), Sn  $3d_{5/2}$  (485.6 eV) and Mn  $2p_{3/2}$  (640.2 eV) indicated the  $\text{In}^{3+}$ ,  $\text{Sn}^{4+}$  and  $\text{Mn}^{2+}$  oxidation states. Magnetic hysteresis loops recorded at 300 K yield a coercivity  $H_c \sim 80$  Oe and saturation magnetization  $M_s \sim 0.39 \mu_B/\text{Mn}^{2+}$  ion. High-temperature magnetometry showed a Curie temperature  $T_c > 600$  K for the 3.2% Mn doped ITO film.

## 1 Introduction

Dilute magnetic semiconductors (DMS) whose lattices are partially substituted by magnetic ions have proven to be very useful in building an all-semiconductor platform for next generation spintronics-based multifunctional devices [1]. To integrate electronics, magnetics and photonics, it is mandatory to develop semiconductors that are not only ferromagnetic at room temperature, but which also have a tunable carrier density, large mobility, high magnetic moment and high optical transparency in order to be used in devices for spin injection and detection. Recently, transition-metal (TM) doped oxide semiconductors such as  $\text{TiO}_2$  [2, 3],  $\text{ZnO}$  [2–7] and  $\text{SnO}_2$  [8–11], have received much attention due to indications suggesting room-temperature ferromagnetism (FM). Such high-temperature FM has been theoretically predicted in many TM doped systems with Mn as one of the favored dopants [12]. The authors [13] have recently observed room-temperature FM in sputter deposited Cr doped  $\text{In}_2\text{O}_3$ . Philip et al. [14] have reported FM in Mn doped indium tin oxide thin films grown on silicon and sapphire substrates by a thermal evaporation process. Their samples showed the anomalous Hall-effect suggesting that this material may be a very promising candidate for spintronics applications. Indium tin oxide (ITO), being a non-stoichiometric n-type wide band gap semiconductor [15] with interesting electrical and optical properties and wide spread applicability [16–18], adds to the interest in developing FM in this material.

In this work, we report the synthesis of ferromagnetic Mn doped ITO films in nanostructured form using an inexpensive sol–gel based chemical method [19, 20]. The samples were investigated using particle induced x-ray emission (PIXE), x-ray diffraction (XRD), spectrophotometry, x-ray photoelectron spectroscopy (XPS), transmission electron

---

K. M. Reddy · J. Hays · A. Punnoose (✉)  
Department of Physics, Boise State University, Boise,  
ID 83725-1570, USA  
e-mail: apunnoos@boisestate.edu

S. Kundu · L. K. Dua · P. K. Biswas  
Sol-gel Division, Central Glass and Ceramic Research Institute,  
Kolkata 700 032, India

C. Wang · V. Shutthanandan · M. H. Engelhard  
Environmental Molecular Sciences Laboratory, Pacific  
Northwest National Laboratory, Richland, WA 99352, USA

X. Mathew  
Centro de Investigación en Energía, Universidad Nacional  
Autonoma de Mexico, Temixco, Morelos 62580, Mexico

microscopy (TEM) and magnetometry, the details of which are given elsewhere [8].

## 2 Experimental results and discussion

XRD patterns of 3.2% and 4% Mn doped ITO deposited on soda lime silica glass, presented in Fig. 1, showed strong peaks of the cubic  $\text{In}_2\text{O}_3$  phase. No separate peaks were observed for  $\text{SnO}_2$ , as the  $\text{In}_2\text{O}_3$  matrix is known to take-up high amounts of Sn [21]. Crystallite sizes estimated from the (222) and (400) lattice planes using the Scherrer equation yield  $16.6 \pm 0.2$  nm and  $17.2 \pm 0.2$  nm for the 3.2% and 4% Mn doped ITO samples respectively. The lattice parameters for the cubic Mn doped ITO system were  $0.998 \pm 0.001$  nm and  $1.004 \pm 0.001$  nm for the 3.2% and 4% Mn doped samples respectively, both of which are lower than the 1.12 nm reported for pure  $\text{In}_2\text{O}_3$  phase [JCPDS Card No. 06-0416]. Such a decrease in the lattice parameter is expected when smaller  $\text{Mn}^{2+}$  and  $\text{Sn}^{4+}$  ions substitute for relatively bigger  $\text{In}^{3+}$  ions [22].

The PIXE data obtained from the two Mn doped ITO samples are shown in Fig. 2. Elemental concentrations were estimated by simulating the experimental PIXE spectra after removing the background due to bremsstrahlung. Respectively, the approximate compositions (Mn:In:Sn) of these samples estimated from the PIXE data were 3.2:88.6:8.2 and 4.0:86.8:9.2.

UV-Vis spectra of the samples (Fig. 3) show a high degree of transmittance ( $\sim 90\%$ ) suggesting that Mn doping

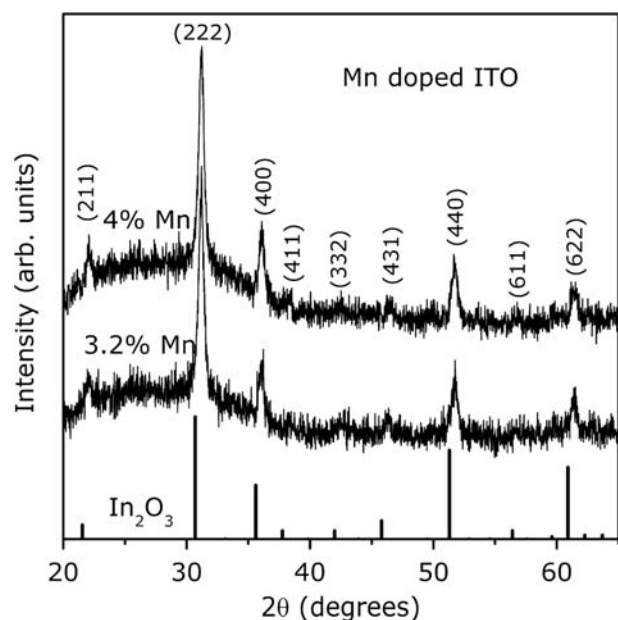


**Fig. 1** X-ray diffraction patterns of 3.2% and 4% Mn doped ITO thin films on soda lime silica glass. The peaks are indexed to the cubic  $\text{In}_2\text{O}_3$  phase

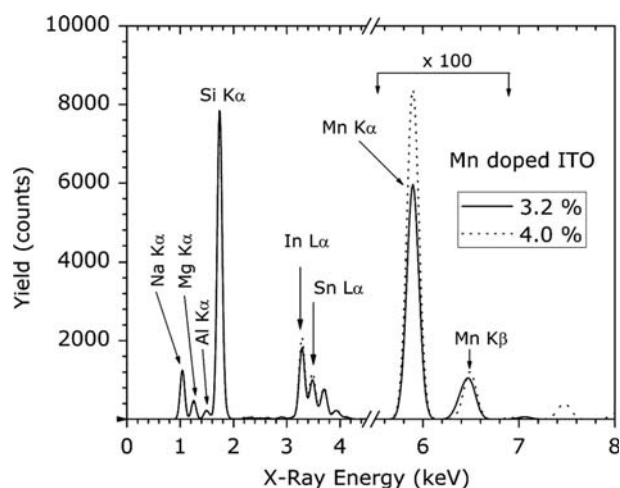


**Fig. 2** Relevant regions of the PIXE spectra obtained from the Mn doped ITO films. Peaks due to Na, Mg, Al and Si are from the silica coated soda lime substrate

does not modify the high transparency of the ITO films. The respective band gap energies of  $3.77 \pm 0.02$  eV and  $3.72 \pm 0.02$  eV, estimated for the 3.2% and 4% Mn doped samples by plotting the absorption coefficient ( $\alpha = -[\ln(T/100)]/t$  (where T is transmittance % and t is the film thickness)) as a function of energy, are comparable to the 3.7 eV reported for pure ITO and are shown in the inset of Fig. 3.

The XPS survey spectrum recorded from the 3.2% Mn doped ITO sample is presented in Fig. 4 along with detailed In, Sn and Mn core binding energy regions shown as insets. XPS concentration estimates obtained using the peak intensities were consistent with the experimental

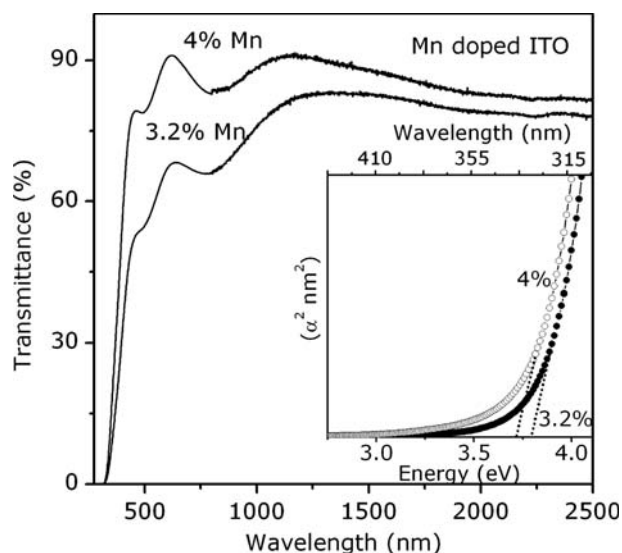


**Fig. 3** The UV-Vis spectra of the Mn doped ITO samples measured in the percentage transmittance mode. The inset shows band gap energy estimates

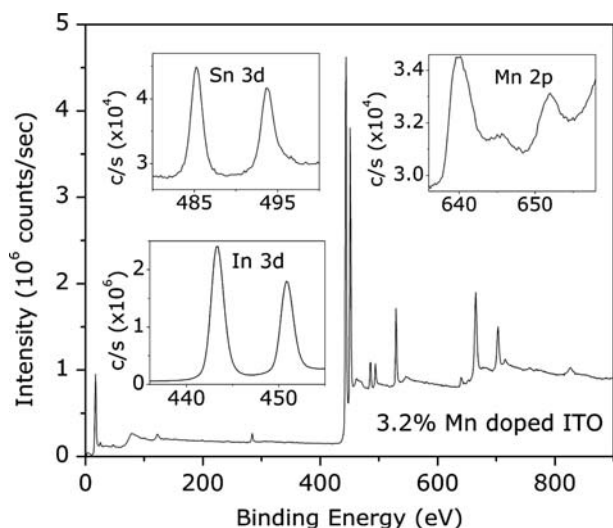


**Fig. 4** XPS survey spectrum of the 3.2% Mn doped ITO film. Insets show detailed In 3d, Sn 3d and Mn 2p regions of the spectrum

doping levels and in reasonable agreement with similar results obtained from PIXE. The observed binding energies for In 3d<sub>5/2</sub>, Sn 3d<sub>5/2</sub> and Mn 2p<sub>3/2</sub> were 443.6, 485.6 and 640.2 eV respectively. These binding energies are comparable to those reported for the In<sup>3+</sup>, Sn<sup>4+</sup> and Mn<sup>2+</sup> states in the literature [23]. The observed binding energy of Mn (640.2 eV) is comparable to that of Mn<sup>2+</sup> in MnS (639.9–640.4 eV). This is possibly due to a similar type of strong hybridization [24] (between the s–p states of the host and the d state of the dopant) in Mn(II) doped ITO that occurs in MnS. However, the binding energy is higher than that of Mn<sup>0</sup> in Mn metal (638.8 eV) and lower than the reported binding energies of Mn<sup>2+</sup> in MnO (641.0 eV), Mn<sup>3+</sup> in Mn<sub>2</sub>O<sub>3</sub> (641.4 eV) and Mn<sub>3</sub>O<sub>4</sub> (641.2 eV), and Mn<sup>4+</sup> in MnO<sub>2</sub> (642.4 eV). Consequently, the presence of any of these Mn oxides in all of the investigated samples is ruled out. This also shows that the chemical environment of the doped Mn ions in the ITO host is different from that of the Mn ions in any of these manganese oxides.

TEM micrographs of the 3.2% and 4% Mn doped ITO films showed nearly spherical nanoparticles with average grain sizes of 16 and 18 nm (see Fig. 5) respectively. High resolution TEM images (Fig. 5b, e) and electron diffraction (ED) patterns (insets of Fig. 5a, e) were collected from several different spots on the same sample to confirm the uniformity in particle size, distribution and crystalline phase which reveals the nanostructured feature of the film. The ED data showed the expected ring patterns for cubic In<sub>2</sub>O<sub>3</sub> with lattice parameter  $a = 1.000 \pm 0.002$  nm, in good agreement with that obtained from XRD. Approximate concentrations of the Mn, In and Sn distributions in the samples, estimated using energy dispersive x-ray analysis (EDX) spectra taken from multiple spots in the

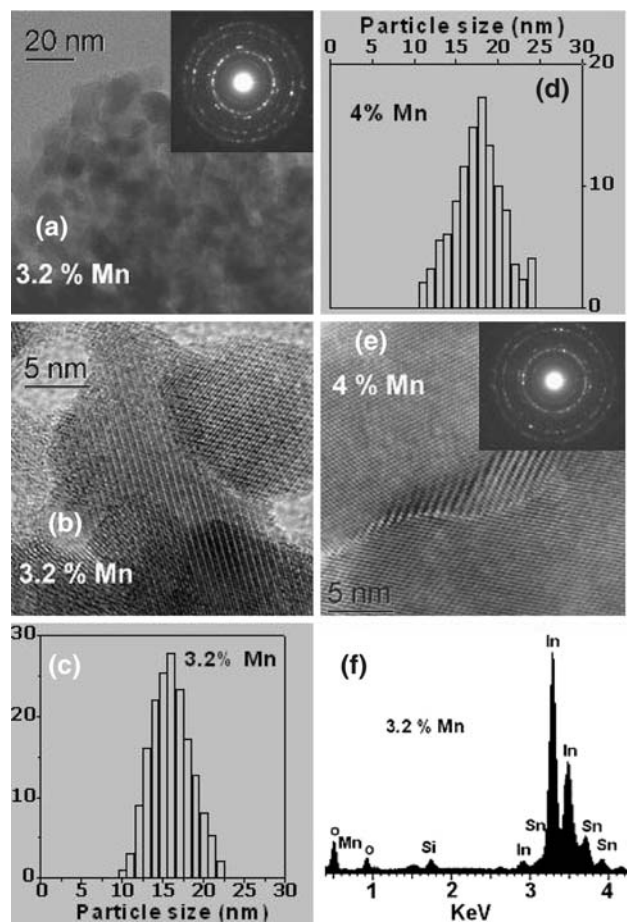


**Fig. 5** (a) and (b) show TEM images of the 3.2% Mn doped sample (inset of (a) shows the electron diffraction pattern), at different resolutions; (c) and (d) show the particle size distribution of 3.2% and 4% Mn doped ITO samples respectively; (e) shows the high resolution TEM image taken from the 4% Mn doped ITO sample with the inset showing the electron diffraction pattern; (f) shows the EDX pattern taken from 3.2% Mn doped ITO film showing well-defined peaks due to In, Mn and Sn

sample (shown in Fig. 5f), were in reasonable agreement with estimates from PIXE studies.

Figure 6 shows a well-defined hysteresis loop obtained from the 3.2% Mn doped ITO sample (volume of the sample film =  $4.25 \times 10^{-5}$  cm<sup>3</sup>) at 300 K with saturation magnetization  $M_s = 14$  emu/cm<sup>3</sup> and coercivity  $H_c \sim 80$  Oe suggesting the presence of a ferromagnetic component in the sample. Assuming that all the doped Mn ions contribute to the FM, this gives a low saturation magnetic moment of  $\sim 0.39 \mu_B/\text{Mn}^{2+}$  ion for the 3.2% Mn doped ITO film. This magnetic moment is only half of the magnitude reported by Philip et al. [14] on Mn doped ITO films deposited using reactive thermal evaporation. The 4% Mn doped ITO film showed a similar hysteresis loop at 300 K but with a much lower  $M_s = 3$  emu/cm<sup>3</sup> and  $H_c \sim 67$  Oe.

Figure 7a shows the magnetization of the 3.2% Mn doped ITO sample measured as a function of temperature  $T$

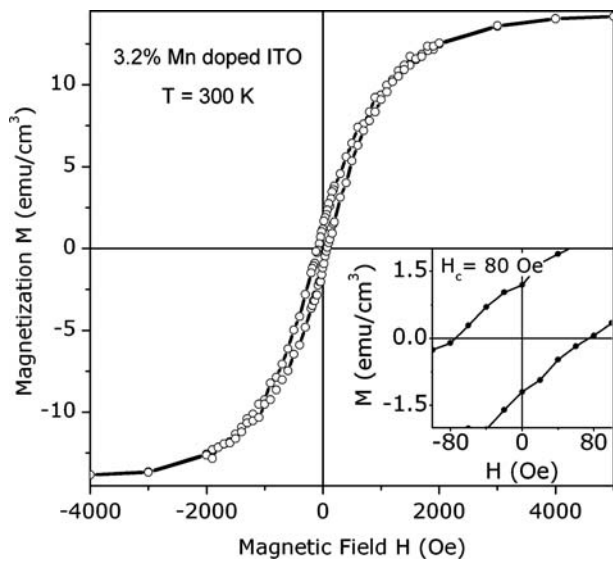


**Fig. 6** Room-temperature hysteresis loop obtained from the 3.2% Mn doped ITO thin film. Inset shows the coercive field

at a constant magnetic field  $H = 8,000$  Oe in the 5–300 K range. The sample magnetization decreases with increasing temperature over this temperature range suggesting that the sample has a strong paramagnetic component in addition to the weak ferromagnetic component as observed in other systems also [10]. The magnetization  $M$  fits reasonably well with the modified Curie–Weiss law

$$\chi = \chi_0 + \frac{C}{T + \theta} \quad (1)$$

where magnetic susceptibility  $\chi = M/H$ ,  $\chi_0 = 1.75 \times 10^{-4}$  emu/cm<sup>3</sup> Oe represents a non-paramagnetic (mostly ferromagnetic) component, Curie constant  $C = n\mu^2/3k_B$  and  $\theta$  is the Curie–Weiss temperature which represents magnetic exchange interactions between the paramagnetic spins,  $n$  number of magnetic ions/g and  $\mu$  is the magnetic moment of the ion. This fit, shown in Fig. 7a, yields  $\theta = 1.094$  K and  $C = 0.00365$  emu K/cm<sup>3</sup> Oe. The presence of a strong paramagnetic component is further confirmed by measuring the  $M$  versus  $H$  variation at 5 K shown as the inset of Fig. 7a. Ignoring the weak ferromagnetic part, this data fits reasonably well with the Brillouin-function-based form for a paramagnetic system, given by

$$M = M_0 \left\{ \left( \frac{2J + 1}{2J} \right) \coth \left[ \frac{(2J + 1)y}{2J} \right] - \left( \frac{1}{2J} \right) \coth \left( \frac{y}{2J} \right) \right\} \quad (2)$$

where  $y = \frac{g\mu_B JH}{kT}$ ,  $M_0$  is the saturation magnetization,  $g$  is the spectroscopic splitting factor ( $g = 2.0023$  for free electrons),  $\mu_B$  is the Bohr magneton and  $k$  is the Boltzmann constant. This fit yields a total angular momentum  $J = 2.80$

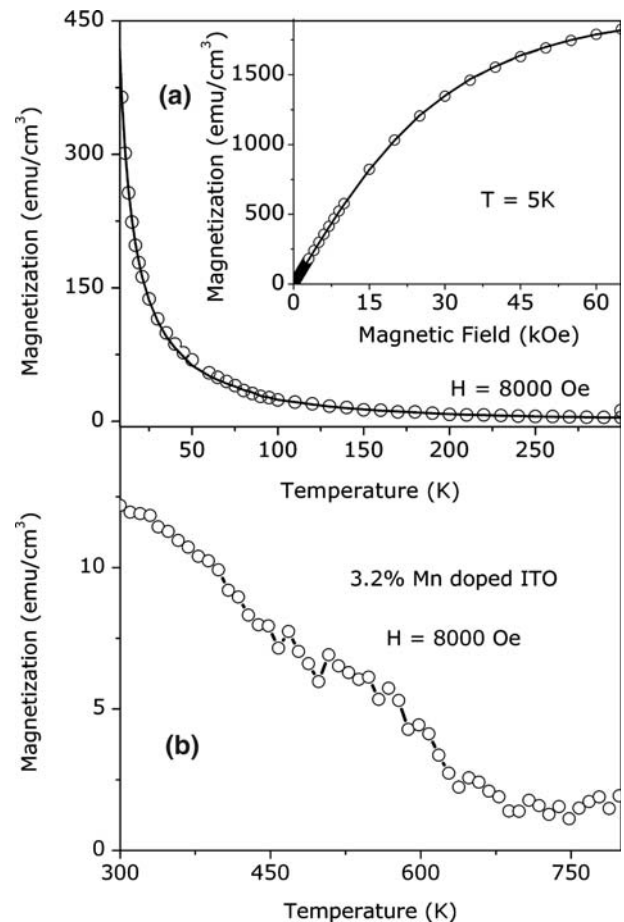


**Fig. 7** Plot showing the variation in the sample magnetization with the temperature of the 3.2% Mn doped ITO film measured with  $H = 8$  kOe using a (a) physical property measurement system in the 5–300 K range and (b) vibrating sample magnetometer in the 300–800 K range. The solid line in the main panel of (a) is a fit using the modified Curie–Weiss law. The inset in (a) shows the  $M$  versus  $H$  data measured at 5 K, along with a fit (solid line) using Eq. 2

and an effective magnetic moment  $p = g[J(J + 1)]^{1/2} = 6.5$ . These values are in reasonable agreement with the expected  $p = 5.9$  for  $Mn^{2+}$  ions with spin  $S = 5/2$  and the 2+ oxidation state indicated from XPS [22, 23]. These results indicating the presence of a strong paramagnetic component in the sample in addition to the weak ferromagnetic part explain the low magnetic moment of  $0.39 \mu_B/Mn^{2+}$  ion in the 3.2% Mn doped ITO film. This value was estimated by assuming that all the dopant ions contribute to the ferromagnetic magnetization, which obviously is not true due to the observed paramagnetic component. Since this moment is less than 10% of the expected magnetic moment for  $Mn^{2+}$  ions, it seems reasonable to assume that probably less than 10% of the doped Mn ions are ferromagnetically coupled in the sample. This is not too unexpected since such low magnetic moments have been reported in a large number of recent studies in TM doped semiconductor oxides [10] in general and in Mn

doped ITO films [15] in particular. Coey et al. [10] have argued that the weak FM observed in transition metal (B) doped semiconductor oxides of the general formula  $(A_{1-x}B_x)(O\phi_\delta)_n$  depends strongly on the doping concentration  $x$  and oxygen vacancy ( $\phi$ ) concentration  $\delta$ . FM in these oxides occur only when  $\delta$  is greater than the polaron percolation limit  $\delta_p$  and  $x$  below its percolation limit of  $x_p$ . According to this model, doped spins in oxides could result in (i) ferromagnetic coupling mediated by shallow donor electrons that form bound magnetic polarons, (ii) antiferromagnetically coupled nearest neighbor cation clusters and (iii) isolated paramagnetic spins. Here ferromagnetic coupling needs the presence of oxygen vacancies in the neighborhood of the dopants, while the latter two result wherever such oxygen vacancies are absent. Since in nanoparticles of semiconductor oxides, oxygen vacancies are most prominent on the surface of the particles and because the surface atomic concentration for 16–18 nm sized particles are close to 10% of the total number of atoms in the particle, the ferromagnetic coupling may be realized primarily on the surface region of the particles. As a result, the oxygen rich core might have dopants existing mostly as isolated paramagnetic ions or antiferromagnetic clusters. Thus, the presence of both ferromagnetic and paramagnetic components in our Mn doped ITO films is qualitative understood based on this model. However, more experimental evidences are necessary to confirm this possibility and will be undertaken in future.

The temperature dependence of the magnetization of the sample above room temperature is shown in Fig. 7b indicating a  $T_c \geq 600$  K due to the ferromagnetic component. Above  $\sim 800$  K, these measurements could not be carried out due to experimental limitations.

### 3 Conclusions

We have demonstrated the development of above room-temperature FM, albeit weak in strength, in spin coated Mn doped transparent ITO thin films with coercivity  $H_c \sim 80$  Oe and saturation magnetization  $M_s \sim 0.39 \mu_B/\text{Mn}^{2+}$  ion. No evidence of any impurity phases were observed in the samples from detailed ED, high-resolution TEM, XPS and magnetometry, suggesting that the observed FM may be intrinsic.

**Acknowledgements** The research work carried out at Boise State University was supported in part by grants from Petroleum Research Fund (AC grant, PRF#41870-AC10), National Science Foundation (DMR-MRI grant; NSF-Idaho-EPSCoR program (EPS-0447689); NSF-CAREER program (DMR-0449639)) and the Department of Energy (DoE-EPSCoR program (DE-FG02-04ER46142)). The support for the work in CGCRI, India was under CTSM program [No. CMM 0022 (1)]. We thank A. Thurber for help with preliminary data

collection. A portion of the research described in this paper was performed in the Environmental Molecular Sciences Laboratory, a national scientific user facility sponsored by the Department of Energy's Office of Biological and Environmental Research and located at Pacific Northwest National Laboratory.

### References

1. H. Ohno, *Science* **281**, 951 (1998)
2. Y. Matsumoto, M. Murakami, T. Shono, T. Hasegawa, T. Fukumura, M. Kawasaki, P. Ahmet, T. Chikyow, S. Koshihara, H. Koinuma, *Science* **291**, 854 (2001)
3. W.K. Park, R.J. Ortega-Hertogs, J.S. Moodera, A. Punnoose, M.S. Seehra, *J. Appl. Phys.* **91**, 8093 (2002)
4. N.S. Norberg, K.R. Kittilstved, J.E. Amonette, R.K. Kukkadapu, D.A. Schwartz, D.R. Gamelin, *J. Am. Chem. Soc.* **126**, 9387 (2004)
5. P.V. Radovanovic, D.R. Gamelin, *Phys. Rev. Lett.* **91**, 157202 (2003)
6. P. Sharma, A. Gupta, K.V. Rao, F.J. Owens, R. Sharma, R. Ahuja, J.M. Osorio Guillen, B. Johanson, G.A. Gerhing, *Nat. Mater.* **2**, 673 (2003)
7. K.R. Kittilstved, D.R. Gamelin, *J. Am. Chem. Soc.* **127**, 5292 (2005)
8. A. Punnoose, J. Hays, V. Shutthanandan, V. Gopal, *Appl. Phys. Lett.* **85**, 1559 (2004); J. Hays, A. Punnoose, R. Baldner, M. Engelhard, J. Peloquin, K.M. Reddy, *Phys. Rev. B.* **72**, 075203 (2005)
9. S.B. Ogale, R.J. Choudhary, J.P. Buban, S.E. Lofland, S.R. Shinde, S.N. Kale, V.N. Kulkarni, J. Higgins, C. Lanci, J.R. Simpson, N.D. Browning, S. Das Sarma, H.D. Drew, R.L. Greene, T. Venkatesan, *Phys. Rev. Lett.* **91**, 077205 (2003)
10. J.M.D. Coey, M. Venkatesan, C.B. Fitzgerald, *Nat. Mater.* **4**, 173 (2005); J.M.D. Coey, A.P. Douvalis, C.B. Fitzgerald, M. Venkatesan, *Appl. Phys. Lett.* **84**, 1332 (2004)
11. H. Kimura, T. Fukumura, M. Kawasaki, K. Inaba, T. Hasegawa, H. Koinuma, *Appl. Phys. Lett.* **80**, 94 (2002)
12. T. Dietl, *Acta Phys. Polon. A* **100**, 139 (2001); T. Dietl, *Semicond. Sci. Technol.* **17**, 377 (2002); T. Dietl, H. Ohno, F. Matsukura, *Phys. Rev. B* **63**, 195205 (2001); T. Dietl, H. Ohno, F. Matsukura, J. Cibert, D. Ferrand, *Science* **287**, 1019 (2000)
13. J. Philip, A. Punnoose, B.I. Kim, K.M. Reddy, S. Layne, J.O. Holmes, B. Satpati, P.R. Leclair, T.S. Santos, J.S. Moodera, *Nat. Mater.* **5**, 298 (2006)
14. J. Philip, N. Theodoropoulou, G. Berera, J. Moodera, B. Satpati, *Appl. Phys. Lett.* **85**, 777 (2004)
15. K.L. Chopra, S. Major, D.K. Pandya, *Thin Solid Films* **102**, 1 (1983)
16. S.A. Bashar, Study on ITO for novel opto electronic devices, A Ph. D. thesis, University of London, 1998
17. P.K. Biswas, A. De, N.C. Pramanik, P.K. Chakraborty, K. Ortner, V. Hock, S. Korder, *Mater. Lett.* **57**, 2326 (2003)
18. P.K. Biswas, A. De, K. Ortner, S. Korder, *Mater. Lett.* **58**, 1540 (2004)
19. K. Tanaka, T. Yoko, M. Atarashi, K. Kamiya, *J. Mater. Sci. Lett.* **8**, 83 (1989)
20. N.C. Pramanik, S. Das, P.K. Biswas, *Mater. Lett.* **56**, 671 (2002)
21. G. McCarthy, J. Welton, *Powder Diffr.* **4**, 156 (1989)
22. R.D. Shannon, C.T. Prewitt, *Acta Crystallogr. Sect. B: Struct. Crystallogr. Cryst. Chem. B* **25**, 925 (1969)
23. C.D. Wagner, J.F. Moulder, L.E. Davis, W.M. Riggs, in *Handbook of X-ray Photoelectron Spectroscopy*, ed. By G.E. Muilenberg (Perkin-Elmer Corporation, Eden Prairie, Minnesota, 1979)
24. A.N.H. Al-Ajili, S.C. Bayliss, *Thin Solid Films* **305**, 116 (1997)